Food Chemistry 315 (2020) 126310

Contents lists available at ScienceDirect

Food Chemistry

journal homepage: www.elsevier.com/locate/foodchem

Polydopamine nanospheres as high-affinity signal tag towards lateral flow immunoassay for sensitive furazolidone detection

Sijie Liu[a,1], Leina Dou[a,1], Xiaolin Yao[a], Wentao Zhang[a], Bingxin Zhao[a], Zonghan Wang[a], Yanwei Ji[a], Jing Sun[b], Baocheng Xu[c], Daohong Zhang[a,*], Jianlong Wang[a,*]

[a] College of Food Science and Engineering, Northwest A&F University, Yangling 712100, Shaanxi, China
[b] Qinghai Key Laboratory of Qinghai-Tibet Plateau Biological Resources, Northwest Institute of Plateau Biology, Chinese Academy of Sciences, Xining 810008, Qinghai, China
[c] College of Food and Bioengineering, Henan University of Science and Technology, Luoyang 471003, China

ARTICLE INFO

Keywords:
Lateral flow immunoassay
Furazolidone
Polydopamine nanospheres
Binding stability

ABSTRACT

Currently, the low sensitivity and poor binding stability of detection probe prepared via electrostatic adsorption have become the dilemmas of colloidal gold-based lateral flow immunoassays (Au-LFIAs). In this connection, polydopamine nanospheres (PDA NPs) with an eminent covalent connectivity property were introduced as a promising substitute to improve the stability of probe and sensitivity of LFIA. Whereafter, the PDA NPs-based LFIA was applied for the monitoring of furazolidone (FZD) in food samples because of the potential carcinogenic/mutagenic effects to human of its metabolite (3-amino-2-oxazolidinone, AOZ). Compared with electrostatic adsorption, the binding stability of PDA NPs-based probes was superior. And, as expected, the PDA NPs-based LFIA biosensor exhibited higher sensitivity than that of the Au-LFIA with a detection limit of 3.5 ng mL^{-1} for AOZ by naked-eye readout. Based on the significant enhanced binding stability and sensitivity, the PDA NPs-based LFIA is of certain spreading value for detecting other analytes.

1. Introduction

Furazolidone, N-(5-nitro-2-furfurylidene)-3-amino-2-oxazolidone (FZD), as one of the most representative nitrofurans antibiotic, is widely used to prevent and treat gastrointestinal infections and other bacterial diseases in animal husbandry (Dou et al., 2018). However, the residue of nitrofurans and their metabolites in foodstuffs would induce carcinogenic and mutagenic effects to human (Le, Xie, Zhu, & Zhang, 2016). Facing with ever-increasing attention for public health and greatly possibilities of FZD contaminated food, a reliable, rapid and highly sensitive detection strategy to protect the health of consumers is important and necessary. Considering FZD could rapidly metabolize into 3-amino-2-oxazolidinone (AOZ) in animal tissues according to its unstable characteristic (Liu et al., 2010), AOZ was often used as a marker for monitoring the presence of FZD. Moreover, the derivative process of AOZ to 3-[(4-carboxyphenyl) monomethyl] amino-2-oxazolidinone (CPAOZ) is a crucial step, because FZD cannot exist in the form of prototype drug and AOZ metabolite must be released from the cellular proteins under mildly acidic conditions (Aldeek, Hsieh, Ugochukwu, Gerard, & Hammack, 2017; Franek et al., 2006).

In response to the enormous perniciousness and extensive accessibility, various diagnostic platforms including liquid chromatography-mass spectrometry (LC-MS) (Kim, Kim, Hyung, Lee, & Kim, 2015), liquid chromatography-tandem mass spectrometry (LC-MS/MS) (Valera-Tarifa, Plaza-Bolaños, Romero-González, Martínez-Vidal, & Garrido-Frenich, 2013) and enzyme-linked immunosorbent assays (ELISA) (Liu et al., 2010) have been established for reliable, reproducible, and sensitive detection of FZD. Although the aforementioned analytical methods offer predominant accuracy and high-throughput screening capability, they are relatively resource demanding and multiple steps of these methods hinders their instant and filed applications. Accordingly, it still remains tremendous requirements to construct facile detection methods with satisfactory sensitivity, simplicity, speed and cost. Lateral flow immunoassay (LFIA), is a paper-based platform that combines the specific response of antigen-antibody and nanomaterials labeling technology to achieve the qualitative and/or quantitative detection of target analytes in intricate matrices. Benefiting from its multiple outstanding advantages such as low cost, results visible by naked eye, small sample volume requirement, shorter detection time, ease of mass production and portability (Cheng, Song, Shi, Du, & Lin, 2019; Quesada-

* Corresponding authors.
E-mail addresses: zhangdh@nwsuaf.edu.cn (D. Zhang), wanglong79@nwsuaf.edu.cn (J. Wang).
[1] Sijie Liu and Leina Dou contributed equally to this work.

https://doi.org/10.1016/j.foodchem.2020.126310
Received 20 September 2019; Received in revised form 21 January 2020; Accepted 27 January 2020
Available online 30 January 2020

González & Merkoçi, 2018), LFIA has now become a most popular and commonly used point-of-care (POC) diagnosis or on-site detection method (Hu et al., 2017; Huang, Aguilar, Xu, Lai, & Xiong, 2016). It must be emphasized that the rapid development of nanomaterials has provided significant power for the progress of LFIAs in various inspection fields, such as medical test (Loynachan et al., 2017), environmental monitoring (Liu et al., 2012) and pesticide residue detection (Liu et al., 2011), especially in the POC inspection of harmful substances in food safety field (Liu et al., 2019; Wang et al., 2019; Yao et al., 2019). Among these, synthesizing intensely colored and biocompatible nanomaterials to label antibodies and be used as probes is one of the core steps in LFIAs for further detection of target analytes (Loynachan et al., 2017).

Unfortunately, it has been reported that noncovalent connection pattern between antibodies and signal tag is not conducive for the stability, repeatability and bonding strength of probes (Lou et al., 2019). On the other hand, conventional covalent attachment which achieved by organic cross-linking agents such as EDC/NHS or glutaraldehyde, may result in the activity reduction or even denaturation of antibodies and thereby affecting the sensitivity (Le et al., 2016; Lou et al., 2018). It is highly desired to find a signal substrate which has several characteristics including strong chroma, biocompatibility, and covalent connectivity (independent of organic reagent) toward antibodies. Over the past decade, mussel-inspired polydopamine (PDA) has showed strongly attachment to almost all types of organic and inorganic substances with high binding strength (Lee, Dellatore, Miller, & Messersmith, 2007). Meanwhile, as a well-known natural melanin, PDA possesses plentiful characteristics, among these, biocompatibility is the most important (Liu, Ai, & Lu, 2014; Simon & Peles, 2010; Xu et al., 2019). Encouragingly, it has been speculated that the oxidized dopamine can conjugate with organic substances via covalent bond formation (Lee, Scherer, & Messersmith, 2006). Furthermore, utilizing the strong quinine-amine group interaction to realize the conjugation strategy between polydopamine and antibodies is more efficient than other chemistry based methods (Wan, Zhang, Wang, Qi, & Hou, 2011). More importantly, polydopamine nanospheres (PDA NPs) possess several additional characteristics including excellent cost effectiveness, aqueous solubility, and strong chroma. Based on these advantages mentioned above, PDA NPs will be one of the best candidates for LFIAs establishment without any doubt.

Herein, a novel LFIA for FZD monitoring was facilely constructed based on high-affinity and biocompatible PDA NPs to solve the mentioned problems, on which the covalent attachment between PDA NPs and Ab was accomplished through facile mixture. Besides, comparative experiment was designed to compare the binding stability of covalent coupling and passive adsorption. Gold nanoparticles (GNPs), the most widely used labeling material in LFIA (Zhang, Li, Zhang, & Zhang, 2011), as the representative of electrostatic adsorption nanomaterials were used to construct GNPs-Ab probes. In order to appraise its feasibility and suitability, the PDA NPs-based LFIA was applied in multiple food samples inclusive of milk powder, pork and shrimp for AOZ residue detection. Results showed that the PDA NPs-based LFIA demonstrated its advantage of simple, sensitive and creditable in this study and has great potential for substituted GNPs based LFIA in POC inspection.

2. Experimental

2.1. Materials and reagents

The anti-CPAOZ antibody was prepared by our laboratory as previously reported (Dou et al., 2019). BSA (CAS: 9048-46-8, purity: > 98%, pH: 6.8-7.2), extracted form bovine blood, was provided by MP Biomedicals (China). AOZ, CPAOZ, lex-dopamine, 4-{[5-(morpholinomethyl)-2-oxooxazolidin-3-ylimino]methyl} benzoic acid (CPAMOZ), clenbuterol hydrochloride, 4-[[2-(aminocarbonyl) hydrazinylidene] methyl]-benzoic acid (CPSEM), chloramphenicol and 1-[(4-Carbo-benzylidene)-amino]-imidazolidin-2,4-dione (CPAHD) were received from Anti Biotechnology. Nitrocellulose (NC) membranes were derived from Millipore Corp. Glass fibers, polyvinyl chloride (PVC) plates, sample and absorbent pads were provided by Shanghai Kingdiag-biotech CO., Ltd. Polyvinylpyrrolidone K-30 (PVP K-30), hydrogen tetrachloroaurate (III) hydrate ($HAuCl_4{\cdot}3H_2O$), 4-carboxybenzaldehyde (4-CBA), polyethylene glycol 20,000 (PEG-20000), dimethyl sulfoxide, polyethylene glycol 2000 (PEG-2000), sucrose, trisodium citrate and sodium azide were purchased from Sigma-Aldrich. Dopamine hydrochloride was purchased from Aladdin. Tween-20, BCA Protein Assay Kit was received from Solarbio. Ethanol, orthoboric acid and ammonia aqueous solution were received from Sinopharm Chemical reagent Co., Ltd. Purified water used in this assay was produced by our laboratory. Skimmed milk powder (fat content: < 1%), red shrimp (about 6 cm) and streaky pork (fat content: 10–30%) used in this work were all purchased from a local supermarket in Yangling, China. And all solvents and other chemicals used in this work were of analytical-reagent grade.

2.2. Apparatus

Dispensing system (HGS510-2D) and Guillotine cutter (HGS-201) were purchased from Hangzhou Autokun Technology Co., Ltd. (Hangzhou, China). The high speed refrigerated centrifuge (HC-3018R) was provided by Anhui USTC Zonkia Scientific Instruments. (Anhui, China). The scanning electron microscopes (SEM) images used to characterize the morphology of PDA NPs were received from the scanning electron microscopes S-4800 (Hitachi, Japan). The Fourier-transform infrared (FT-IR) spectrum was measured using a Vetex 70 (BrukerCorp, Germany) (Zhang, Li, Liu, Yang, & Wang, 2018). The diameter of nanoparticles was evaluated using Zeta sizer Nano-ZS instrument (Malvern, UK). The UV–vis absorption spectra were characterized by a spectrophotometer (UV-2550) (Shimadzu, Japan).

2.3. Synthesis of PDA NPs and GNPs

PDA NPs were synthesized via the oxidation and self-polymerization of dopamine, adapted from the previous work with minor modifications (Liu, Ai, et al., 2013). The volume of ammonia aqueous has an appreciable impact on the size of PDA NPs. Thus, different amounts of ammonia aqueous ranging from 0.4 to 0.8 mL were added into the mixed liquor (8 mL ethanol mixed with 18 mL purified water). After 30 min, 2 mL purified water containing 0.1 g dopamine hydrochloride was quickly injected into the above mixture solution. Accompanying, the color of the solution changed to pale yellow and then gradually turned to deep brown. After 24 h of reaction, PDA NPs were obtained by centrifugation and washing with water for thrice.

The GNPs were prepared via the method reported previously with minor modifications (Zhang et al., 2011). Firstly, different from the literature, 4 mL of 1% trisodium citrate was rapidly added to 100 mL already boiling 0.01% $HAuCl_4{\cdot}3H_2O$ under vigorous stirring. The mixed solution was continuously stirred at boiling temperature and churned for another 15 min after the color was stable. The product was titration to 100 mL by ultrapure water after cooling to room temperature, and then stored at 4 °C for further use. The glass wares used above were all soaked by aqua regia beforehand.

2.4. Preparation of nanoprobes

For the PDA NPs-Ab probe, a typical coupling reaction was carried out. Briefly, 1 mL PDA NPs solution (2.5 mg mL^{-1}) was mixed with 2 μL solution of anti-CPAOZ antibody (1 mg mL^{-1}) and then incubated at room temperature for 1 h. The residual binding sites on PDA NPs surface were blocked by prepared filtered BSA solution with a final concentration of 2%. The mixture was incubated for 3 h at 4 °C, and ultimately the PDA NPs-Ab probes were obtained after twice

centrifugation. Then, nanoprobes were resuspended in 1 mL borate buffer (0.02 M, pH 9.0) containing 0.01% orthoboric acid, 0.1% (w/v) PEG-2000 and 0.02% sodium azide (NaN_3), and then stored at 4 °C for further use.

2.5. Manufacture of the LFIA strip

The LFIA biosensor was made of substrate plate, absorbent pad, NC membrane, conjugate and sample pad. The sample and conjugate pads were dried at 37 °C overnight after treated completely with disparate blocking buffers. The absorbent pad was not treated redundantly. CPAOZ-BSA (0.5 mg mL^{-1}) was dispensed on the NC membrane to construct the test line (T-line) by a jetting rate of 0.8 μL cm^{-1}. The sample and conjugate pad, NC membrane and absorbent pad were orderly assembled onto a plastic adhesive backing card with about 1–2 mm overlapping after completely drying, then the assembled card was cut into strips of 3 mm width and stored in a desiccator.

2.6. Performance of the strip sensor

In order to investigate the performance of this competitive LFIA under optimal conditions, series of detection solutions were prepared by separately mixing 100 μL probe into 0–9 ng mL^{-1} CPAOZ standard solutions. Meanwhile, phosphate buffer saline (PBS, 0.01 M, pH 7.4) was used as the blank control. Subsequently, the detection solution was dripped onto the sample pad of the prepared strip, allowing the liquid to migrate along the strip. The detection result was first observed by naked eyes after 10 min of the reaction, and then recorded via a camera. Finally, Image J software was applied to analyze the signal intensity.

2.7. Detection of CPAOZ in the spiked samples

Milk powder, shrimp and pork confirmed to be free of AOZ by HPLC analysis in advance were used as food samples in this experiment. The pretreatment method of samples was consistent with our previous work (Dou et al., 2019). Firstly, one gram of accurately weighted homogeneous samples (shrimp and pork) and milk powder were first distributed into 10 mL centrifuge tubes by dissolved with ultrapure water respectively. The mixtures were vortexed for a while at room temperature after spiked with AOZ standard solutions. Afterwards, the derivative agent (200 μL of dimethyl sulfoxide containing 0.05 M 4-CBA) was separately added into each sample solution, CPAOZ was derived from AOZ after incubation at 37 °C for 16 h (Fig. S1). Then, the derivative solution supernatant was collected by centrifuged at 10,000 rpm for 10 min, and analyzed in triplicates via the prepared LFIA strips. The blank control assay was carried out to play a role in monitoring the validity of the PDA NPs-based LFIA in each detection.

3. Results and discussion

3.1. Principle of the PDA NPs based competitive LFIA

As illustrated in Fig. 1a, the lateral flow strip composed four parts, including the absorbent pad, the NC membrane of pre-covering CPAOZ-BSA, as well as pretreatment sample and conjugate pads by different running buffers. PDA NPs were used as signal tags in this competition-type immunoreaction. During this assay, sample solution was mixed with PDA NPs probes then the mixture was added to sample pad followed with migration along the sample pad toward absorbent pad driven by the capillary action. Afterwards, the PDA NPs modified antibody could be captured by the pre-coated CPAOZ-BSA on T-line owing to the specific identification reaction. In the wake of the accumulation of probes, the strongest signal was found on T-line when no CPAOZ molecule was present in sample solution. While when CPAOZ existed, a weaker signal would be formed on T-line because of the furious competition between CPAOZ and CPAOZ-BSA for limited probes. In this assay format, the color signal was inversely proportional to the concentration of target analyte in actual samples. When the target concentration was sufficiently high, no significant bands was visible on T-line. Using this format, the result can be observed by naked eyes for semiquantitative analysis and/or recorded by a digital camera for quantitative analysis through Image J software as shown in Fig. 1b.

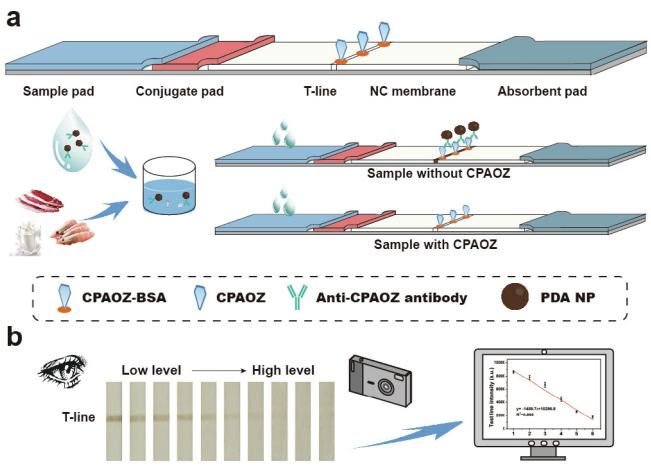

Fig. 1. (a) Schematic illustration of the PDA NPs based LFIA for the detection of CPAOZ. (b) Interpretations of the LFIA results separately achieved by naked eyes for semiquantitative analysis and Image J software for quantitative analysis.

3.2. Characterizations of the PDA NPs and probes

PDA NPs were obtained from the aggregation of monomers via dopamine oxidation and spontaneously self-polymerization without harsh reaction conditions. And the synthesis mechanism of PDA NPs was proposed in Fig. S2, including covalent polymerization and physical self-assembly of dopamine with 5,6-dihydroxyindole (DHI) through oxidation of catechol under an aerobic and alkaline condition (Hong et al., 2012; Liu, Wang, Caro, & Huang, 2013). PDA NPs with various diameter were prepared by adjusting the volume of ammonia aqueous (0.4–0.8 mL). Once the PDA NPs were ready, their morphological information and particle size were provided from the SEM result. In the case where 0.4 mL of ammonia aqueous was added, the diameter of prepared PDA NPs was distributed in 300–400 nm as shown in Fig. S3a and d. With 0.6 mL of ammonia aqueous added, PDA NPs possessed an average diameter of about 250 nm (Fig. S3b and e). When the addition volume of ammonia aqueous was 0.8 mL, the resultant PDA NPs were uniformly spherical in shape with a diameter of 160 nm (Fig. S3c and f). Although increasing the size of nanoparticles could further improve the color intensity of *T*-line, they may also cause false negative results and thus decrease the accuracy of detection. The optimal size of nanoparticles is a balance between brightness and application performance. So, the PDA NPs of last group with an average diameter about 160 nm was selected as the signal tag to further prepare the probe in this work.

Meanwhile, the resultant PDA NPs were uniformly spherical in shape as shown in Fig. 2a. Furthermore, Fig. 2b shows the particle size distribution, the mean diameter of PDA NPs was about 160 nm and the narrow diameter distribution was consistent with the SEM analysis. In order to verify the successful polymerization of dopamine and analyze the chemical structure of PDA NPs, the FT-IR spectra of dopamine and PDA NPs were scanned as shown in Fig. 2c. Dopamine monomers generated a large and broad peak spanning in the 3000–3400 cm^{-1} region, which was attributed to the presence of intermolecular hydrogen bonds in dopamine molecules, double bands at 3353 and 3248 cm^{-1} were ascribed to $-NH_2$ stretching (Zhou, Wang, Lin, Chen, &

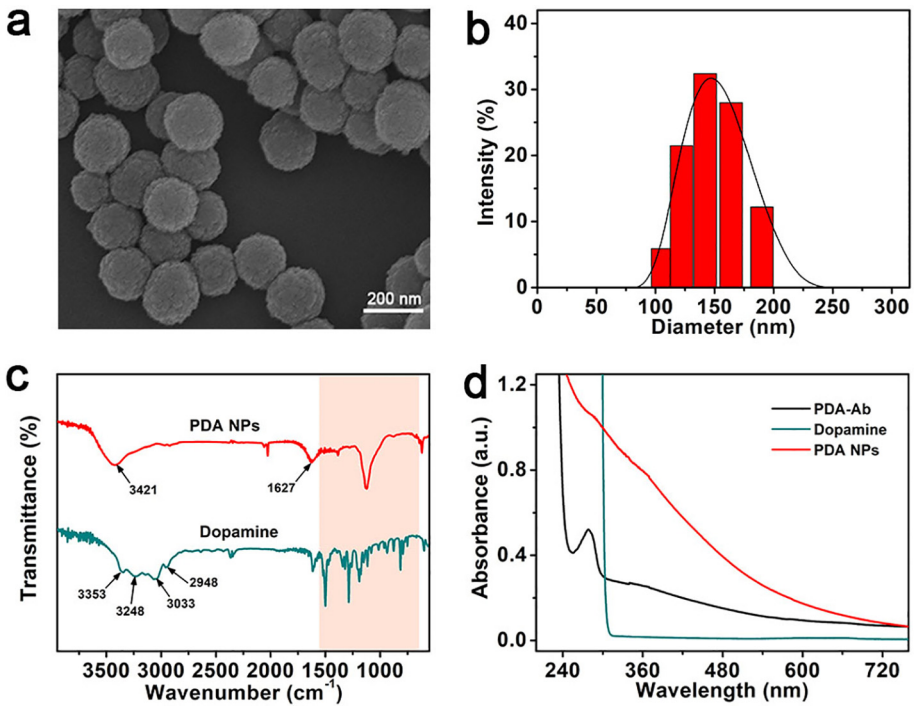

Fig. 2. Characterization of the prepared PDA NPs. (a) SEM image of the prepared PDA NPs, (b) DLS of the synthetic PDA NPs, (c) FT-IR spectroscopies of the PDA NPs (red curve) and dopamine (cyan curve), (d) UV vis spectra of the dopamine (cyan curve), PDA NPs (red curve) and PDA-antibodies (PDA-Ab) probe (black curve). (For interpretation of the references to color in this figure legend, the reader is referred to the web version of this article.)

Yang, 2012). Meanwhile, the characteristic bands at 3145 cm^{-1}, 3061 cm^{-1}, 3033 cm^{-1} and 2944 cm^{-1} were corresponded to the aromatic O—H asymmetry stretching vibration (Gunasekaran, Kumar, & Ponnusamy, 2007). In comparison to corresponding starting materials, the FT-IR spectra of PDA NPs revealed a large and wide band spanning 3200–3600 cm^{-1}, which indicated the existence of a hydroxyl structure (Dreyer, Miller, Freeman, Paul, & Bielawski, 2012). In addition, the peak at 3421 cm^{-1} could be attributed to the stretching vibration of phenolic O—H and N—H, the apparent peak at around 1627 cm^{-1} associated with the bending vibration of N—H and stretching vibration of aromatic ring (Liu, Cao, et al., 2013). What is more, the peak at 1120 cm^{-1} was associated with the N—H shearing vibration of the amide group and the C—O vibration. Simultaneously, the N—H shearing vibrations and stretching of amide group could confirm the appearance of rearrangement reaction and polymerization (Fu et al., 2015). Likewise, as shown in Fig. S4, the disappearance of numerous narrow peaks proved that small molecules were aggregated into PDA NPs. All these results clearly confirmed the successful synthesis of PDA NPs. As presented in Fig. 2d, cyan curve, red curve and black curve respectively represent the UV–Vis Spectra of dopamine, PDA NPs and PDA-Ab probe. Although the spectra of dopamine and PDA NPs were completely different, there was no absorption peak within the measurement range which was also another evidence for the successful synthesis of PDA NPs. Remarkably, a new absorption peak emerged at 280 nm for probes compared to pure PDA NPs owing to the binding of antibodies to PDA NPs which was mainly ascribed to the existence of *ortho*-dihydroxyphenyl functional group in PDA NPs and the strong quinine-amine group interactions between polydopamine and antibody.

3.3. Comparison of different connection patterns between Ab and nanomaterials

PDA NPs were used to construct probes through covalent connection with antibodies, GNPs as the representative of electrostatic adsorption nanomaterial were also used to prepared to GNPs-Ab probe. The connection patterns among PDA NPs-Ab probe (Group 1) and GNPs-Ab probe (Group 2) were compared by the binding stability of Ab and nanomaterials drawing support from a BCA kit detection method. As shown in Fig. 3a, 174.4 ng Ab covalently connected with PDA NPs and 75.7 ng Ab adsorbed on GNPs. The two groups of probes were stored in refrigerator at 4 °C for 5 days and then centrifuged, the supernatants were collected followed separately tested through the BCA kit to quantify the amount of antibody felled off from nanomaterials. Results indicated that 21.2 ng Ab separated from GNPs, which implied that about 28% of Abs felled off in noncovalent connection group (Group 2). Meanwhile, only 15.4% of Abs felled off in Group 1. Contrast experiment proved that the covalent attachment had stronger affinity than that of the electrostatic adsorption between Ab and nanomaterials, which was also consistent with previous research (Lou et al., 2018). Based above, PDA NPs could serve as more excellent signal labels in the LIFAs.

3.4. Optimization of experimental conditions

For the purpose of acquiring the optimal accuracy, sensitivity and lowest background-color of the as-prepared immunosensor, some experimental conditions were investigated. It was worth noting that all experimental operations were performed at room temperature considering the timely and rapid on-site detection requirements. The immobilizing of antibody on carriers with appropriate density was a key parameter to achieve optimum performance. Fig. 3b shows the relationship between analytical performance and different concentrations of PDA NPs. The signal intensity and background-color were gradually enhanced with the addition of PDA NPs concentration under visual conditions. Unfortunately, the higher concentration (3 mg mL^{-1}) of PDA NPs caused hard lateral flow resulting in stronger background interference and decreased signal intensity. Considering the issue, 2.5 mg mL^{-1} of PDA NPs was selected as the optimal condition. The overall performance of the as-prepared immunosensor also closely related to the number of antibodies combined on PDA NPs. On the basis of the selected concentration condition of PDA NPs, the labeling amounts of antibody with a final concentration ranged from 0.5 to 3 μg mL^{-1} were investigated. As displayed in Fig. 3c, the signal intensity on T-line increased by degrees with improve the antibody concentration during 0.5–2 μg mL^{-1} and arrived at summit after 2 μg mL^{-1}. So, 2 μg mL^{-1} of antibody was regarded as the appropriate addition dosage in the PDA NPs solution. In addition, the probe volume used in each test was another important factor since the accumulation quantity of probes on T-

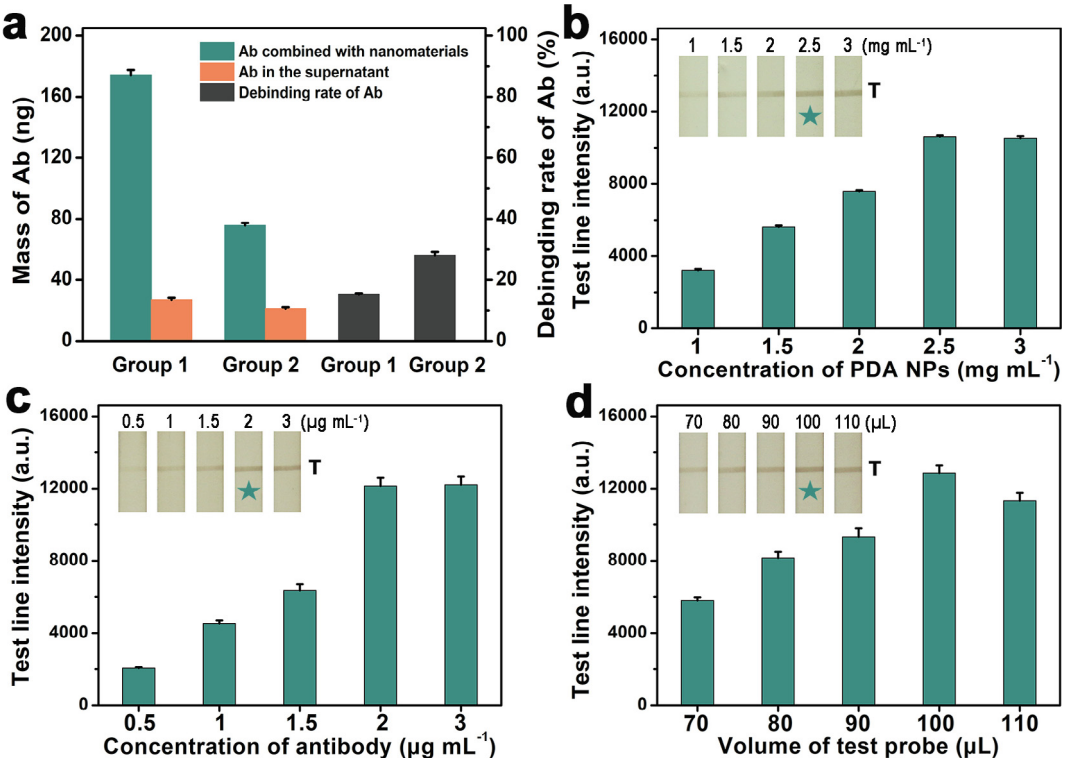

Fig. 3. Binding stability comparison of Ab in two kind probes separately prepared by covalent coupling and electrostatic adsorption. Group 1 represents PDA NPs-Ab probe, Group 2 represents GNPs-Ab probe (a). Optimization results of the labeling concentrations of PDA NPs (b) and anti-CPAOZ antibody (c). Optimization results of the volume of test probe (d). ★ Represents the optimal parameter selected for the following tests.

line could directly affect the signal intensity. As shown in Fig. 3d, compared with the different volumes of test probes, the signal intensity on T-line was heightening followed the increased volume of probe. However, excess volume of probe would result in decreased signal strength and a low sensitivity, and thus was unfavorable for the detection. Considering factors of signal intensity, background interference, detection cost and assay sensitivity, 100 μL was used as the optimal volume of probe.

Besides, aiming at further improving analytical performances, other experimental conditions such as concentration of CPAOZ-BSA, running buffers for sample and conjugate pads and so on were also optimized and summarized in Tables S1 and S2.

3.5. Analytical performance

Sensitivity was an essential factor of point-of-care (POC) equipment. Thus, the sensing performance and dynamic range of the resulting PDA NPs-based LFIA toward CPAOZ inspection were evaluated. To this end, different levels of CPAOZ ranged from 0 to 9 ng mL^{-1} were detected under optimal conditions via the developed LFIA. The corresponding responses of LFIA to target CPAOZ were highlighted in Fig. 4a. When inexistence of CPAOZ, a dark brown band could discover on T-line. The signal intensity was not inhibited in this situation and was regarded as 100% saturation. For the positive samples, the signal response decreased with the faded brown band lines of T-line when CPAOZ concentration was increased. In general, the limit of detection (LOD) was regarded as the minimum concentration of CPAOZ when T-line was invisible by naked eyes. Therefore, the LOD of the proposed biosensor was 8 ng mL^{-1} for CPAOZ, at this concentration the signal intensity analyzed by Image J software was as low as 4.63% of the saturated intensity, which could be regarded as the visual LOD of the LFIA. In order to quantitative analysis the CPAOZ, the mean gray value of optical density in the test zone was calculated by Image J software. The processing procedure was described detailly in Fig. S5. Furthermore, calibration data obtained for each concentration subsequently allowed us to determine the dynamic range and reconfirm the LOD of the assay. The obtained calibration curve indicated that the signal intensity was inversely proportional to the concentration of CPAOZ ranging from 0 to 8 ng mL^{-1}. A good linear relationship with a correlation coefficient of 0.980 between the signal intensity and CPAOZ concentration was plotted in Fig. 4b. The regression equation could be fitted as $y = -1489.7 \times C_{[CPAOZ]} + 10296.8$ with a dynamic range of 1–6 ng mL^{-1}. By calculation, the sensitivity (in the standard samples that caused 10% decrease of the intensity than that produced by the blank control (Zhang, Wang, Chen, Fang, & Yu, 2009)) of the PDA NPs-based LFIA toward CPAOZ detection was 0.69 ng mL^{-1}. Besides, the coefficient of variations (CVs, n = 3) were 2.41%, 4.66%, 5.60%, 6.68%, 4.89%, 12.75%, 11.12%, and 11.26% for 1, 2, 3, 4, 5, 6, 7, and 8 ng mL^{-1} CPAOZ respectively. These results suggested the excellent precision and reproducibility of the immunosensor. Furthermore, the concentration of AOZ could be calculated by CPAOZ using the flowing formula (Yan et al., 2018):

Concentration of AOZ = (molecular weight of AOZ/molecular weight of CPAOZ) × concentration of CPAOZ

Therefore, the visual LOD of AOZ detection based on this method was 3.5 ng mL^{-1}. Specially, compared with colloidal gold based LFIA (electrostatic adsorption) (Xie, Zhang, & Le, 2017) and quantum dot based LFIA (covalent binding by EDC/NHS) (Le et al., 2016), the biosensor proposed (covalent binding without organic reagent) in this work possessed better or comparable analytical performance as shown in Table S3.

In order to investigate the specificity of the PDA NPs-based LFIA, selective experiments were carried out. The potential interfering substances including lex-dopamine, CPAMOZ, clenbuterol hydrochloride, CPSEM, chloramphenicol, and CPAHD, whose structures were given in Fig. S6. As shown in Fig. 4c, it could be clearly observed that all T-line of strips were close to the control strip even though the interfering substances were 100 ng mL^{-1}. However, the deep brown band

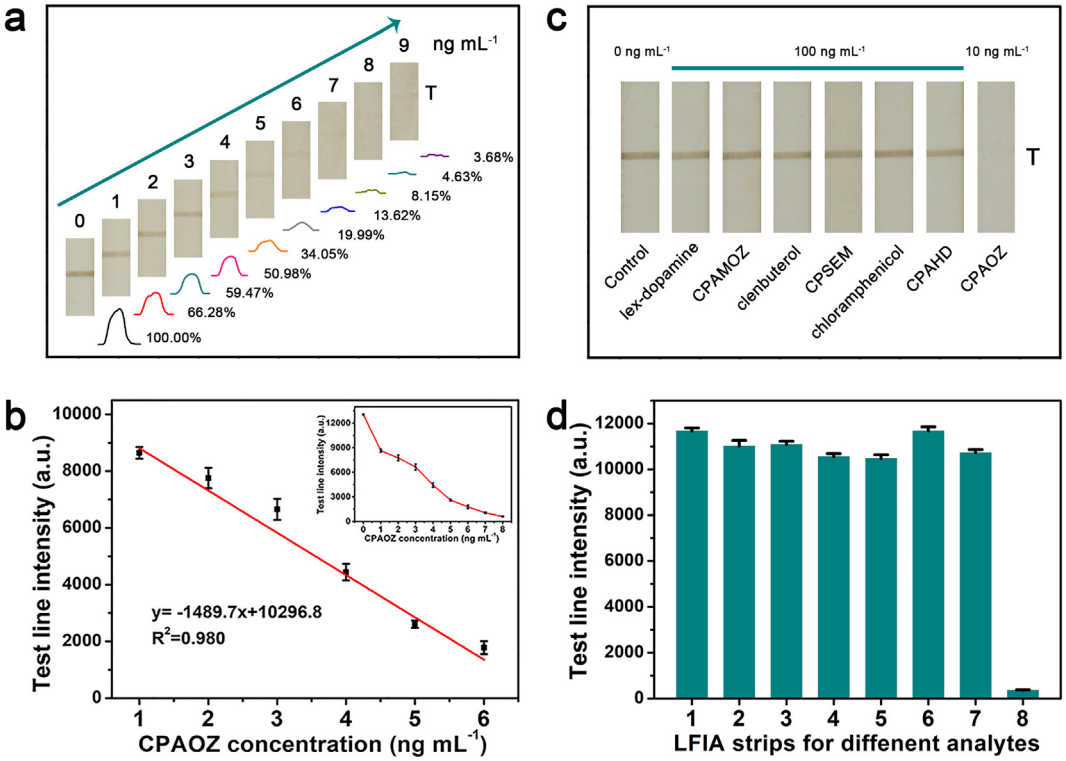

Fig. 4. Assay performances of the PDA NPs-based LFIA for CPAOZ detection. (a) Sensitivity result, the inset percentages represent the corresponding signal intensities on the *T*-line of strips. (b) Calibration curve, the inset shows the variation rule within the whole detection range. (c) Specificity result. (d) Specificity result processed by Image J software, No. 1 corresponds to the control strip, 2–7 correspond to 100 ng mL^{-1} of lex-dopamine, CPAMOZ, clenbuterol hydrochloride, CPSEM, chloramphenicol, and CPAHD, respectively, 8 corresponds to 10 ng mL^{-1} of CPAOZ. Error bars show standard deviations of three replicate measurements.

completely disappeared on T-line for CPAOZ of just 10 ng mL^{-1}. Then, the corresponding mean gray values of optical density in the test zones were calculated using Image J software and demonstrated in Fig. 4d to further clearly exhibit the differences of signal intensities on *T*-line of strips separately for interfering substances and target analyte. The CVs for all results of the specific evaluation experiment were less than 3.5%. Hence, the above results indicated that this analytical method possessed superior specificity toward target analytes.

3.6. Application in actual samples

To access the application performance of the PDA NPs-based LFIA in practical samples, known concentration (1–6 ng mL^{-1}) of AOZ standard solutions were spiked with PBS (0.01 M, pH 7.4) as the blank control. After sample treatment and derivatization, the obtained sample solution was tested using the PDA NPs-based LFIA. All experiments were repeated three times. The semiquantitative detection results in three food samples including milk powder, shrimp and pork were showed in Fig. 5. With the raising of AOZ concentration the brown color faded on T-line. Simultaneously, the detection limits of AOZ in three spiked samples were 5 ng mL^{-1}, 5 ng mL^{-1} and 4 ng mL^{-1} respectively. Compared with experimental theoretical values, the inconsistent of detection limit in actual samples could be ascribed to the complex matrix interference of actual samples. Furthermore, standard addition method was used to evaluate the analytical reliability and accuracy in actual samples by recovery experiments. The results obtained by quantitative analysis were summarized in Table 1. The recoveries of this sensing system ranged from 80.81% to 118.34%. And the CVs (2.38%–7.50%) in three repeated measurements were within the acceptable limit. Furthermore, the application performance for CPAOZ in practical samples (Fig. S7 and Table S3) seeded a little better than that for AOZ. Anyway, all these results demonstrated that this analytical method possessed an acceptable reliability and better potential for future practical application.

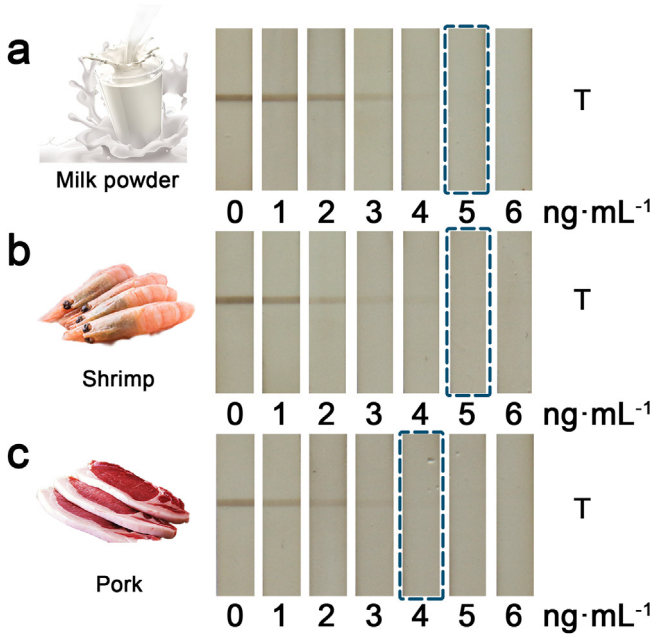

Fig. 5. Detection results of AOZ in milk powder (a), shrimp (b), and pork (c) samples by the PDA NPs-based LFIAs.

4. Conclusions

In summary, PDA NPs were introduced as the signal substrate for the first time to construct a sensitive, effective and simple LFIA. Under optimal conditions, the visual LOD of the PDA NPs-based LFIA for AOZ

Table 1
Recoveries and variation coefficients of the PDA NPsbased LFIA for AOZ determination in spiked samples (n = 3).

Sample	Added (ng mL^{-1})	Found (ng mL^{-1})	Recovery (%)	CV (%)
Milk Powder	1.00	0.86 ± 0.06	85.76	2.88
	2.00	2.08 ± 0.03	103.95	3.27
	3.00	2.61 ± 0.19	90.26	6.22
Shrimp	1.00	0.94 ± 0.05	93.76	2.59
	2.00	1.66 ± 0.10	82.93	7.50
	3.00	2.39 ± 0.09	80.81	6.09
Pork	1.00	1.18 ± 0.04	118.34	2.38
	2.00	1.92 ± 0.06	96.14	5.30
	3.00	2.60 ± 0.11	89.25	6.07

as low as 3.5 ng mL^{-1}, which was possessed better or comparable analytical performance than other LFIAs. Besides, this biosensor demonstrated excellent linear range and satisfying reliability in milk powder, shrimp and pork. Different from widely used GNPs, PDA NPs exhibited a covalent connectivity to antibodies without additional processing in the preparation of NPs-Ab probe, which provided the potential to move toward a simple, high repeatable, and stable LFIA system. In comparison to conventional GNPs-Ab probes, PDA NPs were seized of higher binding efficiency and stability toward Ab. Taken together, all of assessment and application results suggested that the proposed method could be used as a reliable, sensitive referential tool for POC detection of harmful analytes.

CRediT authorship contribution statement

Sijie Liu: Formal analysis, Methodology, Writing - original draft. **Leina Dou:** Formal analysis, Methodology, Writing - original draft. **Xiaolin Yao:** Formal analysis, Conceptualization. **Wentao Zhang:** Formal analysis. **Bingxin Zhao:** Investigation. **Zonghan Wang:** Formal analysis. **Yanwei Ji:** Software. **Jing Sun:** Formal analysis. **Baocheng Xu:** Formal analysis. **Daohong Zhang:** Supervision, Writing - review & editing. **Jianlong Wang:** Supervision, Writing - review & editing.

Declaration of Competing Interest

The authors declare that they have no known competing financial interests or personal relationships that could have appeared to influence the work reported in this paper.

Acknowledgements

The authors thank the National Natural Science Foundation of China (No. 21675127), the Shaanxi Provincial Science Fund for Distinguished Young Scholars (2018JC-011), the Key Research and Development Plan of Shaanxi Province (2019NY-109), the Development Project of Qinghai Provincial Key Laboratory (2017-ZJ-Y10), and the Capacity Building Project of Engineering Research Center of Qinghai Province (2017-GX-G03).

Appendix A. Supplementary data

Supplementary data to this article can be found online at https://doi.org/10.1016/j.foodchem.2020.126310.

References

Aldeek, F., Hsieh, K. C., Ugochukwu, O. N., Gerard, G., & Hammack, W. (2017). Accurate quantitation and analysis of nitrofuran metabolites, chloramphenicol, and florfenicol in seafood by ultrahigh-performance liquid chromatography-tandem mass spectrometry: Method validation and regulatory samples. *Journal of Agricultural and Food Chemistry, 66*(20), 5018–5030.

Cheng, N., Song, Y., Shi, Q., Du, D., & Lin, Y. (2019). Au@Pd nanopopcorn and aptamer nanoflower assisted lateral flow strip for thermal detection of exosomes. *Analytical Chemistry, 91*(21), 13986–13993.

Dou, L., Bu, T., Zhang, W., Zhao, B., Yang, Q., & Huang, L. (2019). Chemical-staining based lateral flow immunoassay: A nanomaterials-free and ultra-simple tool for a small molecule detection. *Sensors and Actuators B: Chemical, 279*, 427–432.

Dou, L., Zhao, B., Bu, T., Zhang, W., Huang, Q., & Yan, L. (2018). Highly sensitive detection of a small molecule by a paired labels recognition system based lateral flow assay. *Analytical and Bioanalytical Chemistry, 410*(13), 3161–3170.

Dreyer, D. R., Miller, D. J., Freeman, B. D., Paul, D. R., & Bielawski, C. W. (2012). Elucidating the structure of poly (dopamine). *Langmuir, 28*(15), 6428–6435.

Franek, M., Diblikova, I., Vass, M., Kotkova, L., Stastny, K., Frgalova, K., & Hruska, K. (2006). Validation of a monoclonal antibody-based ELISA for the quantification of the furazolidone metabolite (AOZ) in eggs using various sample preparation. *Veterinarni Medicina-Praha-, 51*(5), 248.

Fu, J., Chen, Z., Wang, M., Liu, S., Zhang, J., & Zhang, J. (2015). Adsorption of methylene blue by a high-efficiency adsorbent (polydopamine microspheres): Kinetics, isotherm, thermodynamics and mechanism analysis. *Chemical Engineering Journal, 259*, 53–61.

Gunasekaran, S., Kumar, R. T., & Ponnusamy, S. (2007). Vibrational spectra and normal coordinate analysis of adrenaline and dopamine.

Hong, S., Na, Y. S., Choi, S., Song, I. T., Kim, W. Y., & Lee, H. (2012). Non-covalent self-assembly and covalent polymerization co-contribute to polydopamine formation. *Advanced Functional Materials, 22*(22), 4711–4717.

Hu, J., Jiang, Y.-Z., Wu, L.-L., Wu, Z., Bi, Y., & Wong, G. (2017). Dual-signal readout nanospheres for rapid point-of-care detection of ebola virus glycoprotein. *Analytical Chemistry, 89*(24), 13105–13111.

Huang, X., Aguilar, Z. P., Xu, H., Lai, W., & Xiong, Y. (2016). Membrane-based lateral flow immunochromatographic strip with nanoparticles as reporters for detection: A review. *Biosensors and Bioelectronics, 75*, 166–180.

Kim, D., Kim, B., Hyung, S.-W., Lee, C. H., & Kim, J. (2015). An optimized method for the accurate determination of nitrofurans in chicken meat using isotope dilution–liquid chromatography/mass spectrometry. *Journal of Food Composition and Analysis, 40*, 24–31.

Le, T., Xie, Y., Zhu, L., & Zhang, L. (2016). Rapid and sensitive detection of 3-amino-2-oxazolidinone using a quantum dot-based immunochromatographic fluorescent biosensor. *Journal of Agricultural and Food Chemistry, 64*(45), 8678–8683.

Lee, H., Dellatore, S. M., Miller, W. M., & Messersmith, P. B. (2007). Mussel-inspired surface chemistry for multifunctional coatings. *Science, 318*(5849), 426–430.

Liu, X., Huang, L., Wang, Y., Sun, J., Yue, T., Zhang, W., & Wang, J. (2019). One-pot bottom-up fabrication of a 2D/2D heterojuncted nanozyme towards optimized peroxidase-like activity for sulfide ions sensing. *Sensors and Actuators B: Chemical,* 127565.

Lee, H., Scherer, N. F., & Messersmith, P. B. (2006). Single-molecule mechanics of mussel adhesion. *Proceedings of the National Academy of Sciences, 103*(35), 12999–13003.

Liu, C., Jia, Q., Yang, C., Qiao, R., Jing, L., & Wang, L. (2011). Lateral flow immunochromatographic assay for sensitive pesticide detection by using Fe_3O_4 nanoparticle aggregates as color reagents. *Analytical Chemistry, 83*(17), 6778–6784.

Liu, Q., Wang, N., Caro, J., & Huang, A. (2013). Bio-inspired polydopamine: A versatile and powerful platform for covalent synthesis of molecular sieve membranes. *Journal of the American Chemical Society, 135*(47), 17679–17682.

Liu, X., Cao, J., Li, H., Li, J., Jin, Q., & Ren, K. (2013). Mussel-inspired polydopamine: A biocompatible and ultrastable coating for nanoparticles in vivo. *ACS Nano, 7*(10), 9384–9395.

Liu, X., Xiang, J.-J., Tang, Y., Zhang, X.-L., Fu, Q.-Q., & Zou, J.-H. (2012). Colloidal gold nanoparticle probe-based immunochromatographic assay for the rapid detection of chromium ions in water and serum samples. *Analytica Chimica Acta, 745*, 99–105.

Liu, Y., Ai, K., Liu, J., Deng, M., He, Y., & Lu, L. (2013). Dopamine-melanin colloidal nanospheres: An efficient near-infrared photothermal therapeutic agent for in vivo cancer therapy. *Advanced Materials, 25*(9), 1353–1359.

Liu, Y., Ai, K., & Lu, L. (2014). Polydopamine and its derivative materials: Synthesis and promising applications in energy, environmental, and biomedical fields. *Chemical Reviews, 114*(9), 5057–5115.

Liu, Y., Peng, D., Huang, L., Wang, Y., Chang, C., & Ihsan, A. (2010). Application of a modified enzyme-linked immunosorbent assay for 3-amino-2-oxazolidinone residue in aquatic animals. *Analytica Chimica Acta, 664*(2), 151–157.

Lou, D., Fan, L., Cui, Y., Zhu, Y., Gu, N., & Zhang, Y. (2018). Fluorescent nanoprobes with oriented modified antibodies to improve lateral flow immunoassay of cardiac troponin I. *Analytical Chemistry, 90*(11), 6502–6508.

Lou, D., Ji, L., Fan, L., Ji, Y., Gu, N., & Zhang, Y. (2019). Antibody-oriented strategy and mechanism for the preparation of fluorescent nanoprobes for fast and sensitive immunodetection. *Langmuir, 35*(14), 4860–4867.

Loynachan, C. N., Thomas, M. R., Gray, E. R., Richards, D. A., Kim, J., & Miller, B. S. (2017). Platinum nanocatalyst amplification: Redefining the gold standard for lateral flow immunoassays with ultrabroad dynamic range. *ACS Nano, 12*(1), 279–288.

Quesada-González, D., & Merkoçi, A. (2018). Nanomaterial-based devices for point-of-care diagnostic applications. *Chemical Society Reviews, 47*(13), 4697–4709.

Simon, J. D., & Peles, D. N. (2010). The red and the black. *Accounts of Chemical Research, 43*(11), 1452–1460.

Valera-Tarifa, N. M., Plaza-Bolaños, P., Romero-González, R., Martínez-Vidal, J. L., & Garrido-Frenich, A. (2013). Determination of nitrofuran metabolites in seafood by ultrahigh performance liquid chromatography coupled to triple quadrupole tandem mass spectrometry. *Journal of Food Composition and Analysis, 30*(2), 86–93.

Wan, Y., Zhang, D., Wang, Y., Qi, P., & Hou, B. (2011). Direct immobilisation of antibodies on a bioinspired architecture as a sensing platform. *Biosensors and Bioelectronics, 26*(5), 2595–2600.

Wang, Z., Yao, X., Wang, R., Ji, Y., Yue, T., & Sun, J. (2019). Label-free strip sensor based on surface positively charged nitrogen-rich carbon nanoparticles for rapid detection of Salmonella enteritidis. *Biosensors and Bioelectronics, 132*, 360–367.

Xu, S., Zhang, G., Fang, B., Xiong, Q., Duan, H., & Lai, W. (2019). Lateral flow immunoassay based on polydopamine-coated gold nanoparticles for the sensitive detection of zearalenone in maize. *ACS Applied Materials & Interfaces, 11*(34), 31283–31290.

Xie, Y., Zhang, L., & Le, T. (2017). An immunochromatography test strip for rapid, quantitative and sensitive detection of furazolidone metabolite, 3-amino-2-oxazolidinone, in animal tissues. *Food and Agricultural Immunology, 28*(3), 403–413.

Yan, L., Dou, L., Bu, T., Huang, Q., Wang, R., & Yang, Q. (2018). Highly sensitive furazolidone monitoring in milk by a signal amplified lateral flow assay based on magnetite nanoparticles labeled dual-probe. *Food Chemistry, 261*, 131–138.

Yao, X., Wang, Z., Dou, L., Zhao, B., He, Y., & Wang, J. (2019). An innovative immunochromatography assay for highly sensitive detection of 17β-estradiol based on an indirect probe strategy. *Sensors and Actuators B: Chemical, 289*, 48–55.

Zhang, W., Li, S., Liu, X., Yang, C., & Wang, J. (2018). Oxygen-generating MnO2 nanodots-anchored versatile nanoplatform for combined chemo-photodynamic therapy in hypoxic cancer. *Advanced Functional Materials, 28*(13), 1706375.

Zhang, D., Li, P., Zhang, Q., & Zhang, W. (2011). Ultrasensitive nanogold probe-based immunochromatographic assay for simultaneous detection of total aflatoxins in peanuts. *Biosensors and Bioelectronics, 26*(6), 2877–2882.

Zhang, M.-Z., Wang, M.-Z., Chen, Z.-L., Fang, J.-H., & Yu, X.-P. (2009). Development of a colloidal gold-based lateral-flow immunoassay for the rapid simultaneous detection of clenbuterol and ractopamine in swine urine. *Analytical and Bioanalytical Chemistry, 395*(8), 2591.

Zhou, Z., Wang, Q., Lin, J., Chen, Y., & Yang, C. (2012). Nucleophilic addition-triggered lanthanide luminescence allows detection of amines by Eu (thenoyltrifluoroacetone)$_3$. *Photochemistry and Photobiology, 88*(4), 840–843.

Further reading

Zhou, Y., Ding, L. Y., Wu, X., Huang, W., Lai, & Xiong, Y. (2019). Emerging strategies to develop sensitive AuNP-based ICTS nanosensors. *TRAC Trends in Analytical Chemistry, 112*, 147–160.